www.nature.com/cdd

CDDpress

ARTICLE

DNMT1-mediated lncRNA *IFFD* controls the follicular development via targeting *GLI1* by sponging miR-370

Xiaofeng Zhou[1], Yingting He[1], Xiangchun Pan[1], Hongyan Quan[1], Bo He[1], Yongguang Li[1], Guofeng Bai[1], Nian Li[1], Zhe Zhang[1], Hao Zhang[1], Jiaqi Li[1]✉ and Xiaolong Yuan[1]✉

DNA methylation and long noncoding RNAs (lncRNAs) exhibit an indispensable role in follicular development. However, the specific mechanisms regarding lncRNAs mediated by DNA methylation in follicular development remain unclearly. In this study, we found that inhibiting the expression of *DNMT1* promoted granulosa cells (GCs) apoptosis to inhibit follicular development. A novel follicular development-associated lncRNA named inhibitory factor of follicular development (*IFFD*) was mediated by *DNMT1* and showed to arrest follicular development by inhibiting GCs proliferation and estrogen (E2) secretion but promoting GCs apoptosis. Mechanistically, the deactivated Cas9-*TET1* demonstrated that the hypomethylation in −1261/−1254 region of *IFFD* promoted the transcription of *IFFD* by recruiting SP1. *IFFD* induced the expression of GLI family zinc finger 1 through competitive binding miR-370, thereby up-regulating the expression of *CASP3* to promote GCs apoptosis, as well as downregulating the expressions of *PCNA* and *CYP19A1* to inhibit GCs proliferation and E2 secretion. Collectively, *DNMT1*-mediated *IFFD* might be a novel target for the regulation of follicular development.

Cell Death & Differentiation (2023) 30:576–588; https://doi.org/10.1038/s41418-022-01103-y

INTRODUCTION

In mammals, the ovarian follicles normally develop into maturations to ovulate and release a fertilizable oocyte to support generations of species, which is a complex multicellular process controlled by intrafollicular factors and peripheral hormones [1, 2]. The abnormal follicular development leads to a series of serious reproductive diseases such as polycystic ovary syndrome (PCOS) [3, 4], primary ovarian insufficiency [5], and ovarian cancer [6] in humans. Both the arrested follicular development and hyperandrogenism are commonly associated with female infertility, ovulatory dysfunction as well as depression [7]. Primary ovarian insufficiency, the result of follicular dysfunction and depletion, is characterized by the absence of regular menstrual cycles, elevated follicle-stimulating hormone (FSH) and reduced estrogen (E2) concentrations, and usually leads to sterility and reproductive diseases [8, 9]. However, no effective therapy treats and cures these devastating diseases, and the specific regulation mechanism of follicular development remains to be further explored.

As the main supporting cells in follicles, the granulosa cells (GCs) implicate in the follicular development [2, 10]. The increases in proliferation and E2 secretions of GCs significantly promote follicular development, maturation, and ovulation [11, 12], while the increase of GCs apoptosis leads to follicular atresia [13]. Studies have confirmed that DNA methylation [14, 15] and long noncoding RNAs (lncRNAs) [16] are potential therapeutic strategies to control follicular development and ovarian diseases. However, the mechanism that DNA methylation regulates follicular development remains unclear. In mice, 5-azacytidine, a DNA methyltransferase inhibitor [17], results in the obstruction of follicular development [18]. Besides, the DNA methylation of luteinizing hormone receptor gene significantly decreases by equine chorionic gonadotropin (eCG) in mice, a universal induction of follicular development [19]. Moreover, eCG treatment decreases the methylation status at promoters in approximately 40% of genes in GCs with the reduction of *Dnmt1* at S phase [20]. Furthermore, we have found that the hypomethylation of *RSPO2* promoter regulates the apoptosis and proliferation of GCs to control follicular development in pigs [10]. LncRNAs, defined as non-coding RNAs with transcripts over 200 nucleotides [21], have participated in numerous biological processes by acting as competing endogenous RNAs (ceRNAs) [22, 23]. In PCOS patients, lncRNA *MALAT1* sponges miR-125b and miR-203a to promote GCs apoptosis [24], LINC-01572:28 blocks GCs growth by reducing the degradation of p27 [25], and lnc-MAP3K13-7:1 inhibits GCs proliferation through downregulating *DNMT1* expression and the hypomethylation of *CDKN1A* promoter [26], thereby blocking the follicular development and ovulation. Silencing lncRNA *NEAT1* causes defects in corpus luteum formation [27], and decreases the fertility in mice [28]. These results indicate that DNA methylation and lncRNAs may directly target GCs function to regulate follicular development, but the molecular mechanism has not been largely explored.

In this study, using a well-established DNA methyltransferase inhibitor 5-Aza-CdR to treat porcine GCs, we found a novel

[1]Guangdong Laboratory of Lingnan Modern Agriculture, National Engineering Research Center for Breeding Swine Industry, Guangdong Provincial Key Lab of Agro-Animal Genomics and Molecular Breeding, College of Animal Science, South China Agricultural University, Guangzhou, Guangdong, China. ✉email: jqli@scau.edu.cn; yxl@scau.edu.cn

Edited by M. Hardwick

Received: 8 April 2022 Revised: 14 November 2022 Accepted: 1 December 2022
Published online: 24 December 2022

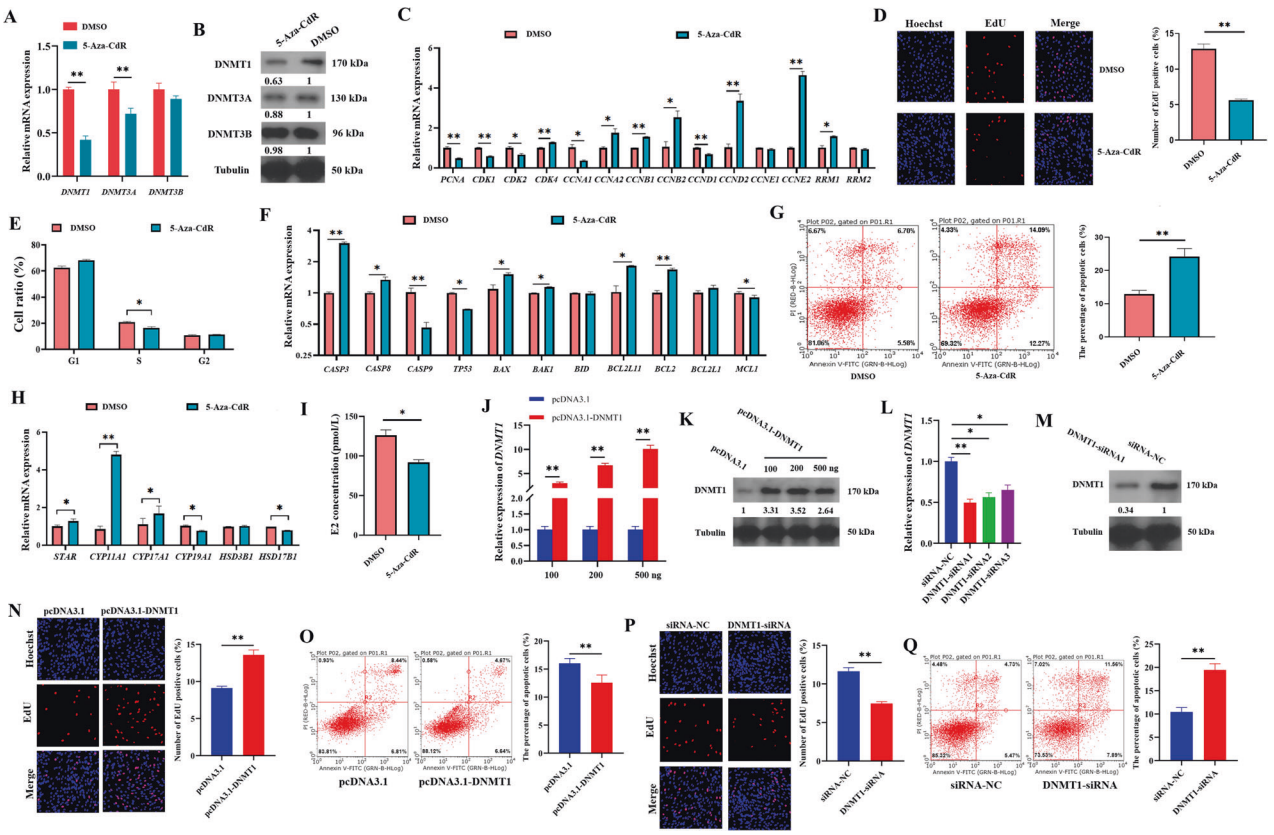

Fig. 1 *DNMT1* regulates the proliferation and apoptosis of GCs. Effect of 5-Aza-CdR on the mRNA (**A**) and protein (**B**) levels of *DNMT1*, *DNMT3A* and *DNMT3B* in porcine GCs. **C** Effect of 5-Aza-CdR on the mRNA levels of genes related to cell cycle in GCs. Effect of 5-Aza-CdR on GCs proliferation detected by EdU (**D**) and flow cytometry (**E**). Effect of 5-Aza-CdR on the mRNA levels of apoptosis-related genes (**F**) and GCs apoptosis (**G**). Effect of 5-Aza-CdR on the mRNA levels of E2 secretion-related genes (**H**) and the E2 concentration (**I**) in GCs. Effect of pcDNA3.1-*DNMT1* (**J**, **K**) or *DNMT1*-siRNA (**L**, **M**) on the expression of *DNMT1* in GCs. The proliferation (**N**) and apoptosis (**O**) rates of GCs after transfection with pcDNA3.1-*DNMT1*. The proliferation (**P**) and apoptosis (**Q**) rates of GCs after transfection with *DNMT1*-siRNA. * indicates $P < 0.05$, ** indicates $P < 0.01$.

follicular development-associated lncRNA named inhibitory factor of follicular development (*IFFD*), which was mediated by *DNMT1*. Furthermore, *IFFD* increased the expression of GLI family zinc finger 1 (*GLI1*), an essential mediator of Hedgehog signaling pathway [29], by sponging miR-370 to promote GCs apoptosis, inhibit GCs proliferation and E2 secretion, and then ultimately regulate the follicular development. Our results provide new insights regarding the therapeutic benefit of *DNMT1*-mediated lncRNAs into follicular development.

RESULTS

DNMT1 regulates the proliferation and apoptosis of GCs

5-Aza-CdR was utilized to explore DNA methylation on the biological effects of GCs, and it was found that the viability (Fig. S1A) and number (Fig. S1B) of GCs treated with 5-Aza-CdR were notably declined in a dose-dependent manner. Also, 5-Aza-CdR significantly decreased the mRNA levels of *DNMT1* and *DNMT3A* in GCs for 24 h (Fig. S1C) and 48 h (Fig. S1D) in a dose-dependent, but exhibited an insignificant influence on *DNMT3B*. To reduce the toxic effect of 5-Aza-CdR on GCs, 0.5 μM was selected for further using, and it was likely to perform the best at 24 h (Fig. S1E). We found that 5-Aza-CdR prominently declined the mRNA and protein levels of *DNMT1* (Fig. 1A, B). Although the mRNA level of *DNMT3A* was significantly inhibited, the protein level was not markedly changed, and 5-Aza-CdR displayed an insignificant effect on *DNMT3B* expression (Fig. 1A, B). 5-Aza-CdR prominently declined the mRNA levels of *PCNA*, *CDK1*, *CDK2*, *CCNA1*, and *CCND1*, but significantly elevated the mRNA levels of *CDK4*, *CCNA2*, *CCNB1*, *CCNB2*, *CCND2*, *CCNE2*, and *RRM1* of cell cycle signaling pathway (Fig. 1C). Moreover, 5-Aza-CdR significantly inhibited GCs proliferation (Fig. 1D) and reduced the number of cells in S phase (Fig. 1E). Besides, 5-Aza-CdR prominently elevated the mRNA levels of *CASP3*, *CASP8*, *BAX*, *BAK1*, *BCL2L11*, and *BCL2*, but inhibited the mRNA levels of *CASP9*, *TP53*, and *MCL1* of apoptosis signaling pathway (Fig. 1F). Flow cytometry (Fig. 1G) further confirmed that 5-Aza-CdR significantly facilitated GCs apoptosis. Besides, 5-Aza-CdR notably elevated the mRNA levels of *STAR*, *CYP11A1*, and *CYP17A1*, but declined the mRNA levels of *CYP19A1* and *HSD17B1* of Estrogen signaling pathway (Fig. 1H), and significantly inhibited E2 secretion (Fig. 1I). Therefore, 5-Aza-CdR might inhibit GCs proliferation and E2 secretion, but promote GCs apoptosis by decreasing the expression of *DNMT1*.

To explore the role of *DNMT1* in GCs, the *DNMT1* overexpression plasmid (pcDNA3.1-*DNMT1*) and *DNMT1* small interfering RNA (*DNMT1*-siRNA) were built. The mRNA and protein levels of *DNMT1* in GCs were enhanced markedly with pcDNA3.1-*DNMT1*, and 500 ng of pcDNA3.1-*DNMT1* showed the greatest overexpression effect (Fig. 1J, K). Three *DNMT1*-siRNAs (*DNMT1*-siRNA1, *DNMT1*-siRNA2, and *DNMT1*-siRNA3) were synthesized, and *DNMT1*-siRNA1 notably declined the mRNA and protein levels of *DNMT1* with the strongest knockdown efficiency (Fig. 1L, M). Although the effects of pcDNA3.1-*DNMT1* (Fig. S1F) and *DNMT1*-siRNA1 (Fig. S1G) on the *DNMT1* expression were in a time-dependent manner, 24 h was selected for further using. EdU staining (Fig. 1N) and flow cytometry (Fig. 1O) showed that pcDNA3.1-*DNMT1* significantly

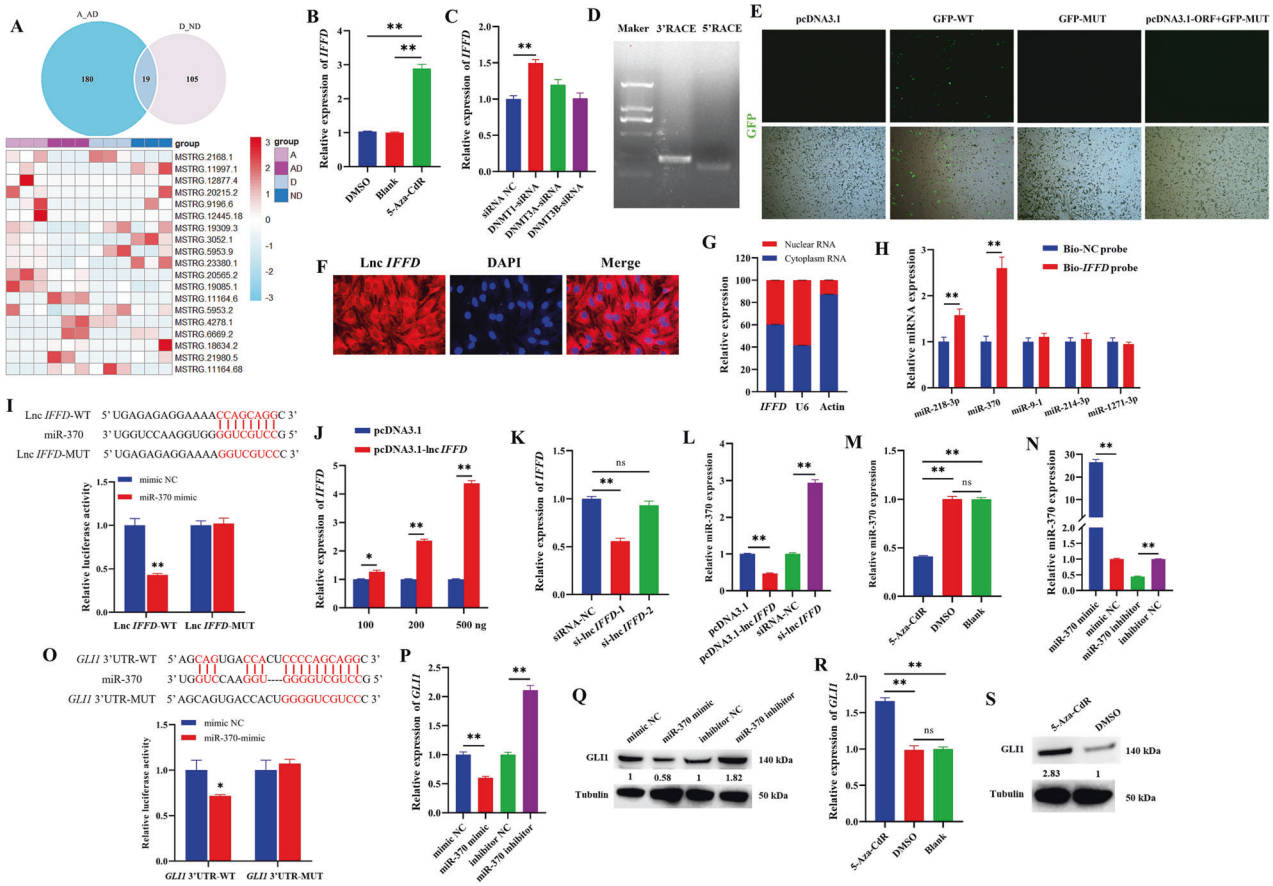

Fig. 2 *DNMT1*-mediated the expression of *IFFD* as ceRNA for miR370-*GLI1* in GCs. A Venn plots and heat maps of overlapped differentially expressed lncRNAs between 5-Aza-CdR vs. DMSO and *DNMT1*-siRNA vs. siRNA-NC. The expression of *IFFD* in GCs treated with 5-Aza-CdR (**B**) or *DNMT1*-siRNA, *DNMT3A*-siRNA and *DNMT3B*-siRNA (**C**). **D** Results of *IFFD* 5′ RACE and 3′ RACE. **E** GFP fluorescence was conducted after 48 h transfection with the plasmids. The distribution of *IFFD* in the cytoplasm and nuclei of GCs was determined by FISH (**F**) and qRT-PCR (**G**). U6 and Actin were used as nuclear and cytosolic controls, respectively. **H** The expressions of the five predicted miRNAs bound to *IFFD* in the *IFFD* pull-down complex. **I** Potential binding sites of miR-370 and *IFFD*, and dual-luciferase reporting assay after co-transfection of wild-type/mutant *IFFD* and miR-370 mimic/mimic NC. The overexpression (**J**) and interference (**K**) efficiency of *IFFD*. **L** Effect of pcDNA3.1-lnc *IFFD* or si-lnc *IFFD* on miR-370 expression in GCs. **M** Effect of 5-Aza-CdR on miR-370 expression in GCs. **N** Overexpression and interference efficiency of miR-370. **O** The potential binding sites of miR-370 and *GLI1*, and dual-luciferase reporting assay after co-transfection of wild-type/mutant *GLI1* and miR-370 mimic/mimic NC. Effect of miR-370 mimic or miR-370 inhibitor on the mRNA (**P**) and protein (**Q**) levels of *GLI1*. Effect of 5-Aza-CdR on the mRNA (**R**) and protein (**S**) levels of *GLI1*. * indicates $P < 0.05$, ** indicates $P < 0.01$. In **A**, A represents 5-Aza-CdR group, AD represents DMSO group, D represents *DNMT1*-siRNA group, and ND represents siRNA-NC group.

promoted GCs proliferation and inhibited GCs apoptosis. Conversely, *DNMT1*-siRNA significantly inhibited GCs proliferation (Fig. 1P) and promoted GCs apoptosis (Fig. 1Q). The testosterone (T) is a substrate for E2 synthesis of GCs, and FSH facilitates the proliferation of GGs [30]. To confirm the roles of 5-Aza-CdR and *DNMT1* in GCs under physiological conditions, the GCs were co-cultured with FSH and T. FSH + T significantly elevated the proliferation and E2 synthesis of GCs, and 5-Aza-CdR or *DNMT1*-siRNA made a significant decline in the proliferation and E2 synthesis aroused by FSH + T, but pcDNA3.1-*DNMT1* recovered the declined effects caused by 5-Aza-CdR or *DNMT1*-siRNA (Fig. S2A, B). The effects of FSH + T on apoptosis were also arrested by 5-Aza-CdR or *DNMT1*-siRNA in GCs (Fig. S2C). Therefore, these observations suggested that *DNMT1* might promote GCs proliferation, but inhibit GCs apoptosis.

DNMT1-mediated the expression of *IFFD* as ceRNA for miR-370-*GLI1* in GCs

The RNA-seq data of GCs treated with 5-Aza-CdR (Group A), DMSO (Group AD), *DNMT1*-siRNA (Group D), and siRNA-NC (Group ND) were further obtained, and 19 overlapping differential expression lncRNAs were found between 5-Aza-CdR vs. DMSO and *DNMT1*-siRNA vs. siRNA-NC (Fig. 2A). Among these 19 lncRNAs, MSTRG.2168.1, whom we named *IFFD*, upregulated both in 5-Aza-CdR and *DNMT1*-siRNA groups (Fig. 2A). The qRT-PCR further validated that 5-Aza-CdR (Fig. 2B) and *DNMT1*-siRNA (Fig. 2C) significantly upregulated the expression of *IFFD*. The 5′ and 3′ ends of *IFFD* were obtained through a rapid amplification of cDNA ends (RACE) system (Fig. 2D). We found that *IFFD* located at chr1:268891238-268891653 and was 395 nt in length (accession number OM105888 in NCBI), which comprised of 2 exons. The pcDNA3.1, GFP-WT, GFP-MUT, and pcDNA3.1-ORF with GFP-MUT vectors were transfected into GCs to explore the coding potential of *IFFD*. Compared with GFP-WT, the pcDNA3.1-ORF with GFP-MUT didn't show GFP fluorescence (Fig. 2E), indicating that *IFFD* had no protein-encoding potential. Besides, *IFFD* was found to be predominantly expressed in the cytoplasm by using FISH (Fig. 2F) and nuclear mass separation assay (Fig. 2G). Otherwise, the oocyte-secreting factors GDF9 and BMP15 are essential for normal follicular development [20]. We found that GDF9 + BMP15 significantly declined *IFFD* expression (Fig. S3A) but elevated the mRNA level of *DNMT1* (Fig. S3B). Moreover, FSH + T prominently declined *IFFD* expression (Fig. S3A).

Using online software, *IFFD* was predicted to harbor the target sites of miR-218-3p, miR-370, miR-9-1, miR-214-3p, and miR-1271-

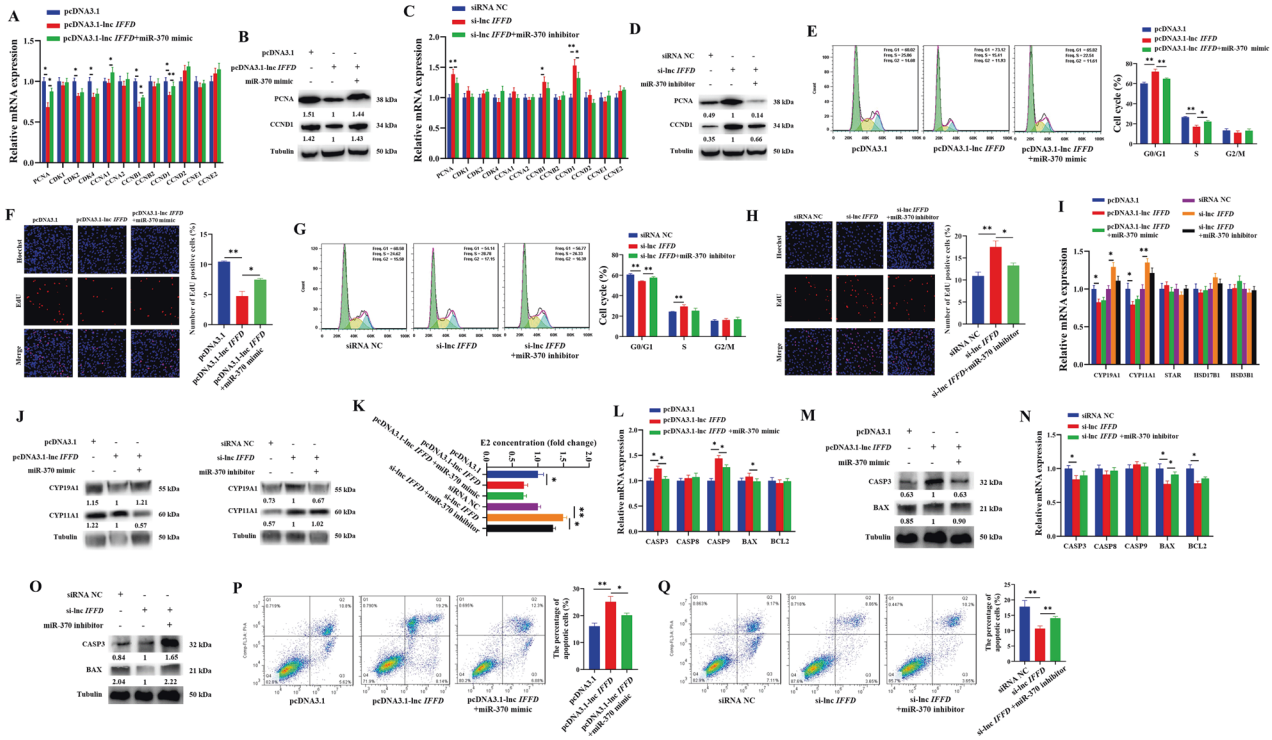

Fig. 3 *IFFD* as ceRNA for miR-370-*GLI1* regulates the proliferation and apoptosis of GCs. Effects of pcDNA3.1-lnc *IFFD* and miR-370 mimic on the mRNA (**A**) and protein (**B**) levels of cell cycle-related genes. Effects of si-lnc *IFFD* and miR-370 mimic on the mRNA (**C**) and protein (**D**) levels of cell cycle-related genes. Effects of pcDNA3.1-lnc *IFFD* and miR-370 mimic on GCs cycle (**E**) and proliferation (**F**). Effects of si-lnc *IFFD* and miR-370 mimic on GCs cycle (**G**) and proliferation (**H**). Effects of *IFFD* and miR-370 on the mRNA (**I**) and protein (**J**) levels of E2 secretion-related genes. **K** Effects of *IFFD* and miR-370 on the E2 secretion of GCs. Effects of pcDNA3.1-lnc *IFFD* and miR-370 mimic on the mRNA (**L**) and protein (**M**) levels of apoptosis-related genes. Effects of si-lnc *IFFD* and miR-370 mimic on the mRNA (**N**) and protein (**O**) levels of apoptosis-related genes. Effects of *IFFD* and miR-370 on GCs apoptosis (**P**, **Q**). * indicates $P < 0.05$, ** indicates $P < 0.01$.

3p. Using RNA pull down, we found miR-370 expression was predominant at the *IFFD* probe group (Fig. 2H). Moreover, the interfering effect of miR-370 on the transcription activity of *IFFD* was restored by mutating the binding site of miR-370 on *IFFD* (Fig. 2I). Figure 2J and Fig. 2K showed that pcDNA3.1-lnc *IFFD* and si-lnc *IFFD*-1 significantly promoted and inhibited the expression of *IFFD*, respectively. The pcDNA3.1-lnc *IFFD* significantly inhibited the expression of miR-370, while si-lnc *IFFD* notably elevated the expression of miR-370 (Fig. 2L). Figure 2M showed that 5-Aza-CdR notably inhibited miR-370 expression. MiR-370 mimic and miR-370 inhibitor notably increased and decreased the expression of miR-370 (Fig. 2N), respectively. The interfering effect of miR-370 on the luciferase activity of *GLI1* was restored by mutating the binding site of miR-370 (Fig. 2O). MiR-370 mimic prominently declined the expression of *GLI1*, while miR-370 inhibitor notably elevated the expression of *GLI1* (Fig. 2P, Q). Alternatively, 5-Aza-CdR prominently promoted the expression of *GLI1* (Fig. 2R, S). These observations showed that *DNMT1*-mediated the expressions of *IFFD*-miR370-*GLI1* axis in GCs.

IFFD as ceRNA for miR-370-*GLI1* regulates the proliferation and apoptosis of GCs

PcDNA3.1-lnc *IFFD* declined the expressions of *PCNA* and *CCND1*, and this inhibitory effect was partially weakened by miR-370 mimic (Fig. 3A, B). Similarly, si-lnc *IFFD* elevated the expressions of *PCNA* and *CCND1*, and this stimulative effect was partially attenuated by miR-370 inhibitor (Fig. 3C, D). The pcDNA3.1-lnc *IFFD* significantly reduced the proportion of GCs at S phase (Fig. 3E), inhibited GCs proliferation (Fig. 3F), and miR-370 mimic partially attenuated these effects. Conversely, si-lnc *IFFD* significantly increased the proportion of GCs at S phase (Fig. 3G), promoted GCs proliferation (Fig. 3H), and miR-370 inhibitor partially attenuated these effects. The pcDNA3.1-lnc *IFFD* declined the expression of *CYP19A1* (Fig. 3I, J) as well as E2 concentration in GCs (Fig. 3K), but si-lnc *IFFD* exhibited the opposite effects. Besides, pcDNA3.1-lnc *IFFD* elevated the expressions of *CASP3* and *BAX*, and this stimulative effect was partially weakened by miR-370 mimic (Fig. 3L, M). Si-lnc *IFFD* declined the expression of *BAX*, and miR-370 inhibitor partially attenuated this inhibitory effect (Fig. 3N, O). The pcDNA3.1-lnc *IFFD* significantly promoted GCs apoptosis (Fig. 3P), while si-lnc *IFFD* significantly inhibited GCs apoptosis, and miR-370 inhibitor partially weakened this inhibitory effect (Fig. 3Q). These results indicated that *IFFD* sponged miR-370 to inhibit the cell cycle, proliferation as well as E2 secretion, but promote the apoptosis of GCs.

To investigate whether *GLI1* participated in the miR-370 mediated mechanism involved in GCs, miR-370 mimic/inhibitor and *GLI1*-siRNA were co-transfected into GCs, respectively. Figure S4A showed that *GLI1*-siRNA1 performed the highest inhibitory effect on the expression of *GLI1*. The qRT-PCR (Fig. S4B) showed that miR-370 mimic promoted the mRNA levels of *PCNA*, *CCNB1*, and *CCND1*, while miR-370 inhibitor inhibited the mRNA levels of *PCNA*, *CCNB1*, and *CCND1*. MiR-370 mimic increased the proportion of GCs at S phase (Fig. S4C), and significantly promoted GCs proliferation (Fig. S4D). Conversely, miR-370 inhibitor reduced the proportion of GCs at S phase and significantly inhibited GCs proliferation, and *GLI1*-siRNA partially attenuate this effect (Fig. S4C, D). Moreover, miR-370 mimic promoted the mRNA level of *HSD17B1*, while miR-370 inhibitor inhibited the mRNA levels of *CYP19A1* and *CYP11A1* (Fig. S4E). ELISA (Fig. S4F) showed that miR-370 inhibitor significantly decreased E2 concentration in GCs, and *GLI1*-siRNA partially attenuated this effect. Besides, miR-370 mimic significantly decreased the mRNA level of *CASP3*, while miR-370 inhibitor significantly elevated the mRNA levels of *CASP3*, *CASP8*,

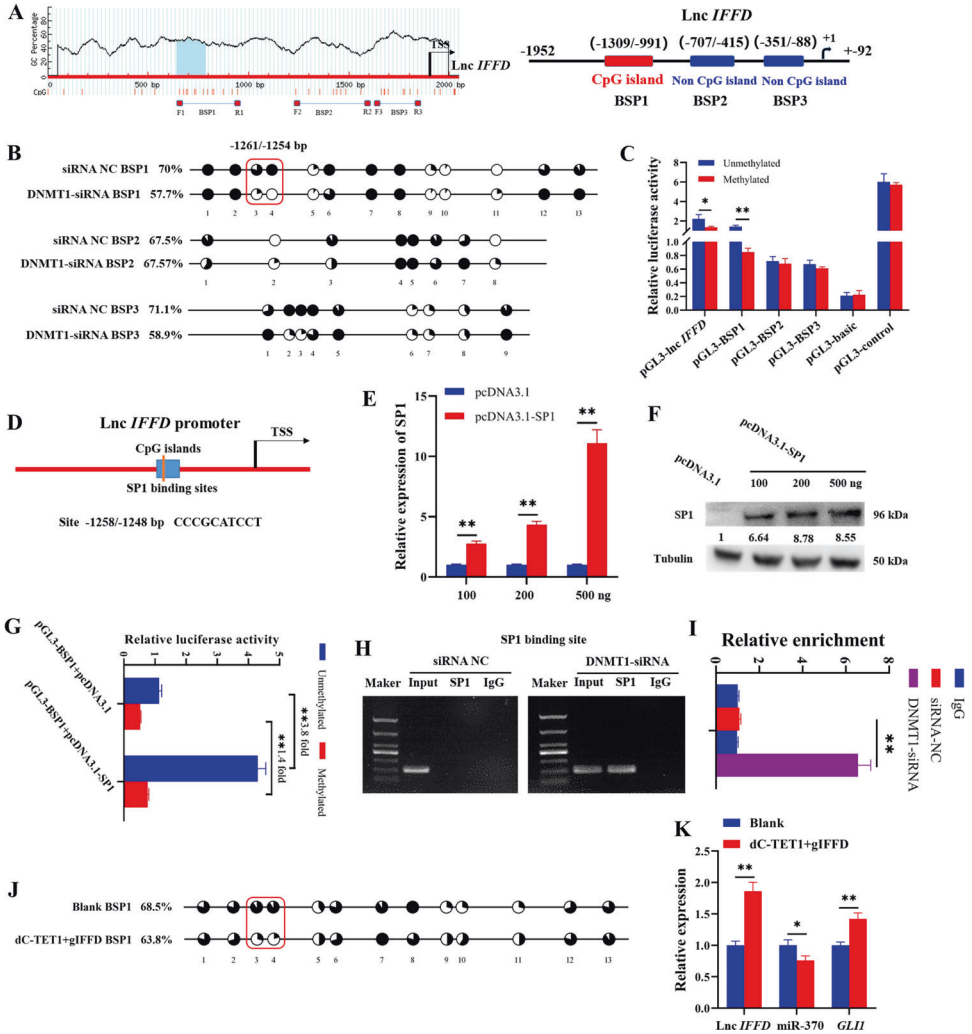

Fig. 4 ***DNMT1* blocks the binding of SP1 to inhibit the transcription of *IFFD*.** **A** Schematic diagram of the CpG island (CGI) at *IFFD* promoter. Blue region represents CGI, and the red column represents bisulfite primers. **B** The methylation status of CGI (BSP1) and non-CGI (BSP2 and BSP3) at the *IFFD* promoter in GCs with *DNMT1*-siRNA. **C** Relative luciferase activity of *IFFD* promoter at different regions methylated in vitro. **D** The SP1-binding sites predicted in the CGI region of *IFFD* promoter. The mRNA (**E**) and protein (**F**) levels of SP1 in GCs transfected with pcDNA3.1-SP1. **G** Effect of pcDNA3.1-SP1 on the luciferase activity of CGI methylated in vitro. Effect of *DNMT1*-siRNA on the enrichment of SP1 at CGI was detected by ChIP-PCR (**H**) and ChIP-qPCR (**I**). **J** The methylation status of CGI (BSP1) in GCs transfected with dC-*TET1* and g*IFFD*. **K** The expressions of *IFFD*, miR-370, and *GLI1* in GCs transfected with dC-*TET1* and g*IFFD*. The red boxes represent potential binding sites of SP1. * indicates $P < 0.05$, ** indicates $P < 0.01$.

and *BAX* (Fig. S4G). Flow cytometry (Fig. S4H) showed that miR-370 mimic notably inhibited GCs apoptosis, while miR-370 inhibitor significantly promoted GCs apoptosis, and *GLI1*-siRNA partially attenuated this effect. These results demonstrated that miR-370 targeted *GLI1* to promote GCs proliferation and E2 secretion, but inhibit GCs apoptosis.

DNMT1 blocks the binding of SP1 to inhibit the transcription of *IFFD*

There was one CpG island (CGI) in the promoter of *IFFD* (named as BSP1, 319 bp in length, −1309 to −991 bp, transcription start site = +1) (Fig. 4A). To explore the DNA methylation-mediated mechanism for the transcription of *IFFD*, the methylation levels of BSP1, BSP2 (293 bp in length, −707 to −415 bp, non-CGI region) and BSP3 (264 bp in length, −351 to −88 bp, non-CGI region) were detected after the treatment of *DNMT1*-siRNA in GCs (Fig. 4A). Compared to the control, the methylation statuses of BSP1 and BSP3 regions were respectively reduced from 70 and 71.1% to 57.7 and 58.9% by *DNMT1*-siRNA, but it was not changed in BSP2 (Fig. 4B). Moreover, the unmethylated pGL3-BSP1 significantly promoted the dual-luciferase activity of *IFFD*, compared with the methylated pGL3-BSP1 (Fig. 4C). But the methylated or unmethylated of pGL3-BSP2 and pGL3-BSP3 did not show significant effect on the luciferase activity of *IFFD* (Fig. 4C). These observations confirmed that the methylation of BSP1 markedly regulated the transcription of *IFFD*.

Furthermore, the PROMO website predicted that there was a potential binding site of SP1 in the −1261 to −1254 region (Fig. 4D). To determine the role of SP1 on the transcription of *IFFD*, the overexpression plasmid of *SP1* (pcDNA3.1-SP1) was built, and pcDNA3.1-SP1 notably elevated the expression of *SP1* (Fig. 4E, F). Compared with the control group, pcDNA3.1-SP1 significantly induced the dual-luciferase activity of unmethylated pGL3-BSP1 by 3.8 times, while only increasing the activity of methylated pGL3-BSP1 by 1.4 times (Fig. 4G). Results of ChIP and ChIP-qPCR showed that *DNMT1*-siRNA obviously promoted SP1 binding in the −1261 to −1254 region (Fig. 4H, I). Moreover, compared to the control, the deactivated Cas9-*TET1* and g*IFFD* vector obviously reduced the methylation status of the SP1-binding site on BSP1 (Fig. 4J), but significantly enhanced the expressions of *IFFD* and

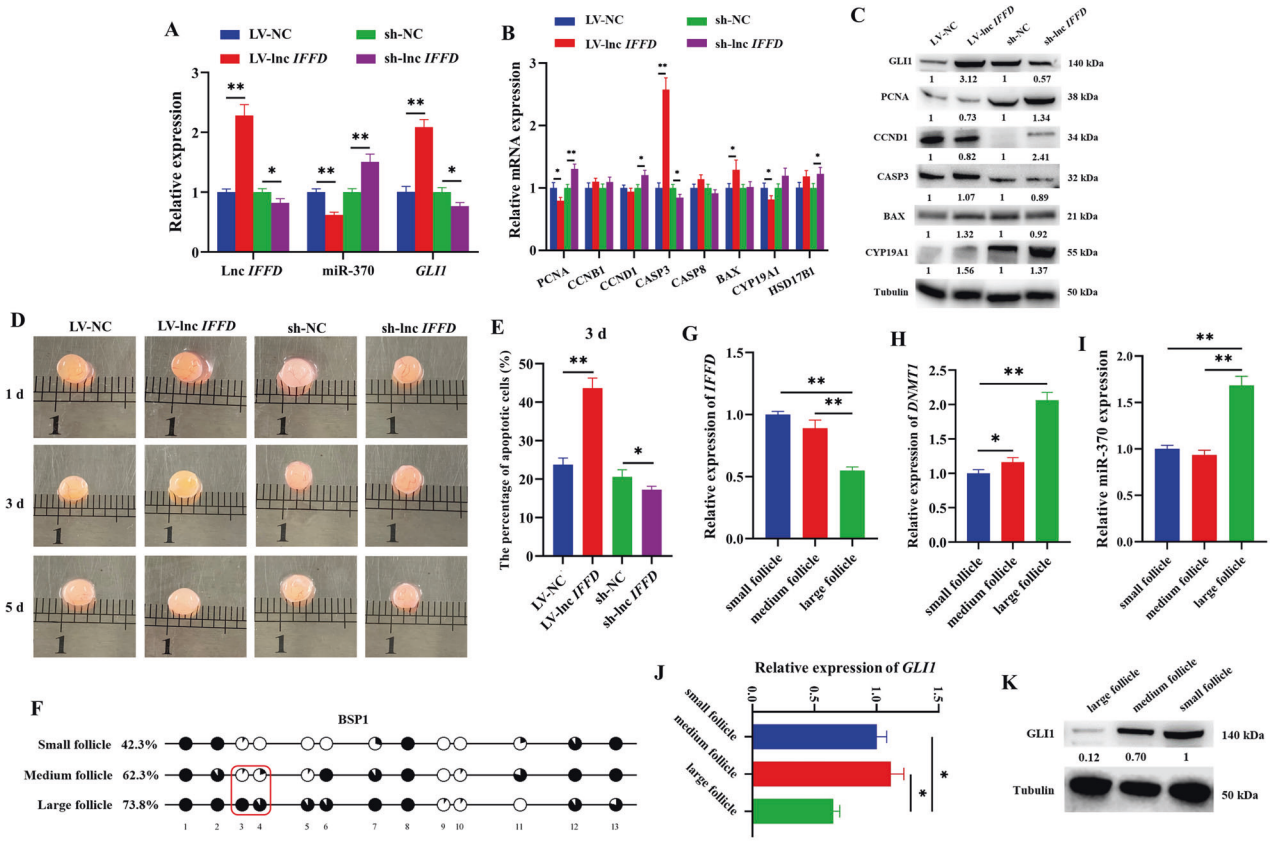

Fig. 5 *IFFD* as ceRNA for miR-370-*GLI1* regulates follicular development in pigs. The mRNA (**A**, **B**) and protein (**C**) levels of *IFFD*, miR-370, *GLI1*, *PCNA*, *CCND1*, *CASP3*, *BAX*, and *CYP19A1* in the porcine follicles transfected with LV-lnc *IFFD* or sh-lnc *IFFD*. **D** The appearance of porcine follicles after transfected with LV-lnc *IFFD* or sh-lnc *IFFD* on the 1st, 3rd, and 5th day. **E** The apoptosis of follicular GCs after transfecting with LV-lnc *IFFD* or sh-lnc *IFFD* on the 3rd day. **F** The methylation level of CGI (BSP1) in small, medium, and large follicles detected by bisulfite sequencing PCR. The expressions of *IFFD* (**G**), *DNMT1* (**H**), miR-370 (**I**) and *GLI1* (**J**, **K**) in small, medium, and large follicles. * indicates $P < 0.05$, ** indicates $P < 0.01$.

GLI1, while decreasing miR-370 expression (Fig. 4K). These results suggested that *DNMT1* induced hypermethylation of *IFFD* and then inhibited its transcription by blocking the binding of SP1.

IFFD as ceRNA for miR-370-*GLI1* regulates follicular development in pigs

To explore the function of *IFFD* on follicular development, LV-lnc *IFFD* or sh-lnc *IFFD* was infected into porcine follicles in vitro. Two days after transfection, the expressions of *IFFD*, miR-370, *GLI1*, *PCNA*, *CCNB1*, *CCND1*, *CASP3*, *CASP8*, *BAX*, *CYP19A1*, and *HSD17B1* were measured. LV-lnc *IFFD* significantly induced the mRNA expressions of *IFFD* and *GLI1*, but significantly inhibited the expression of miR-370 (Fig. 5A). Meanwhile, sh-lnc *IFFD* significantly declined the mRNA expressions of *IFFD* and *GLI1*, but significantly elevated the expression of miR-370 (Fig. 5A). In addition, the expression of *CASP3* significantly increased in follicles infected LV-lnc *IFFD*, but significantly decreased in follicles infected sh-lnc *IFFD* (Fig. 5B, C). The expressions of *PCNA* and *CYP19A1* significantly reduced in follicles infected LV-lnc *IFFD*, but significantly elevated in follicles infected sh-lnc *IFFD* (Fig. 5B, C). Moreover, LV-lnc *IFFD* promoted the turbidity of follicular fluid, the degeneration of blood vessels (Fig. 5D), and the apoptosis of GCs (Fig. 5E), while sh-lnc *IFFD* significantly inhibited GCs apoptosis (Fig. 5E).

Furthermore, in the normal follicles of pigs, the DNA methylation level of BSP1 increased gradually with follicular development (Fig. 5F), the mRNA level of *IFFD* significantly decreased (Fig. 5G), and the mRNA level of *DNMT1* significantly increased (Fig. 5H). The expression of miR-370 notably elevated in large follicles (Fig. 5I), and the expression of *GLI1* prominently declined in large follicles compared with small and medium follicles (Fig. 5J, K). These results suggested that the hypomethylation of *IFFD* might promote GCs apoptosis to inhibit the development of porcine follicles.

IFFD as ceRNA for miR-370-*Gli1* controls follicular development in mice

Using FISH, we found that *IFFD* was widely expressed in different follicular stages in blank mice (Fig. 6A). To further explore the biological function of *IFFD* on follicular development in vivo, LV-lnc *IFFD* or sh-lnc *IFFD* was infected into mouse ovaries. We found that LV-lnc *IFFD* notably elevated the expressions of *IFFD* and *Gli1*, and significantly inhibited the expression of miR-370 (Fig. 6B). However, sh-lnc *IFFD* notably declined the expressions of *IFFD* and *Gli1*, and prominently elevated the expression of miR-370 (Fig. 6B). The expression of *Casp3* significantly increased in ovaries infected LV-lnc *IFFD*, but significantly decreased in ovaries infected sh-lnc *IFFD* (Fig. 6C, D). The expressions of *Pcna* and *Cyp19a1* significantly reduced in ovaries infected LV-lnc *IFFD*, but significantly elevated in ovaries infected sh-lnc *IFFD* (Fig. 6C, D). Moreover, LV-lnc *IFFD* significantly delayed the age of pubertal initiation compared to LV-NC (48.8 ± 2.68 d vs. 38.4 ± 2.07 d, $P < 0.01$, $n = 5$), while sh-lnc *IFFD* markedly shortened the age of pubertal initiation, compared to sh-NC (35 ± 3.08 d, vs. 40.4 ± 1.14 d, $P < 0.01$, $n = 5$) (Fig. 6E). Furthermore, LV-lnc *IFFD* significantly decreased E2 concentration, while sh-lnc *IFFD* significantly increased E2 concentration (Fig. 6F). The LV-lnc *IFFD* significantly increased the number of pre-antrum follicles and antrum follicles, but significantly decreased the number of corpus luteum, and the sh-lnc *IFFD* significantly increased the number of corpus luteum (Fig. 6G). Furthermore, TUNEL determined

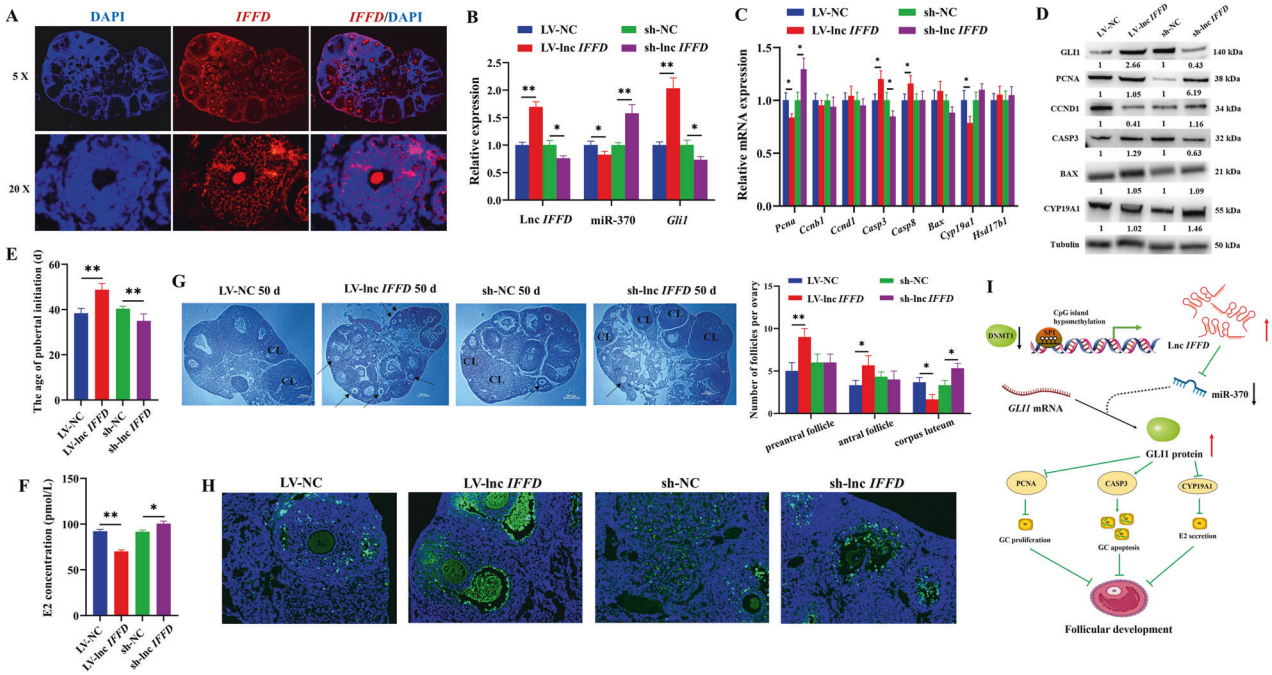

Fig. 6 ***IFFD* as ceRNA for miR-370-*Gli1* controls follicular development in mice. A** The expression and localization of *IFFD* in ovaries detected by FISH. The mRNA (**B**, **C**) and protein (**D**) levels of *IFFD*, miR-370, *Gli1*, *Pcna*, *Ccnd1*, *Casp3*, *Bax*, and *Cyp19a1* in mouse ovary transfected with LV-lnc *IFFD* or sh-lnc *IFFD*. **E** The age of pubertal initiation in mice after ovarian transfection with LV-lnc *IFFD* and sh-lnc *IFFD*. The E2 concentration in serum (**F**), follicular statistics (**G**), and GCs apoptosis (**H**) of 50-day-old mice after ovarian transfection with LV-lnc *IFFD* and sh-lnc *IFFD*. **I** The mechanistic scheme of *DNMT1*-mediated DNA hypomethylation of *IFFD* to block follicular maturation. * indicates $P < 0.05$, ** indicates $P < 0.01$.

that LV-lnc *IFFD* obviously increased GCs apoptosis, but sh-lnc *IFFD* inhibited GCs apoptosis (Fig. 6H and Fig. S5).

DISCUSSION

DNA methylation has been reported to participate in follicular development. Lomniczi et al. used 5-azacytidine to inhibit DNA methylation in rats and found that the ovaries of 5-azacytidine-treated rats had antral follicles, but no corpora lutea, and the rats treated with 5-azacytidine had failed to ovulation [18]. However, Lomniczi *et al*. [18] focused on the regulations of DNA methylation in the hypothalamus. It is not clear how DNA methylation disturbed the follicular development. In our study, 5-Aza-CdR was found to inhibit GCs proliferation (Fig. 1D) and E2 secretion (Fig. 1I), and promote GCs apoptosis in pigs (Fig. 1G). Moreover, *DNMT1* was found to increase GCs proliferation (Fig. 1N) and decrease GCs apoptosis (Fig. 1O). In line with previous studies that 5-Aza-CdR may inhibit proliferation and facilitate apoptosis by reducing *DNMT1* expression in colon cancer cell lines [31], as well as that *DNMT1* downregulation inhibits GCs proliferation and growth by increasing cyclin-dependent kinase inhibitor 1A expression [26].

To explore how DNA methylation involved in follicular development, we analyzed the transcriptomes of porcine GCs treated with 5-Aza-CdR and *DNMT1*-siRNA (Fig. 2A), and found that both 5-Aza-CdR (Fig. 2B) and *DNMT1*-siRNA (Fig. 2C) significantly increased the expression of *IFFD*. In addition, GDF9 + BMP15 prominently declined the expression of *IFFD* (Fig. S3A) but elevated the mRNA level of *DNMT1* (Fig. S3B), and FSH + T prominently declined the expression of *IFFD* (Fig. S3A), indicating the potential roles of *DNMT1* and *IFFD* in the regulation of follicular development. Moreover, we also found a negative correlation between *IFFD* (Fig. 5G) and *DNMT1* (Fig. 5H) expression during normal follicular development in pigs. Therefore, we hypothesized that *DNMT1* might be involved in follicular development by regulating *IFFD* expression.

Similar to protein-coding genes, the expressions of lncRNAs are also regulated by epigenetics [32, 33]. To determine the mechanism of *IFFD* during follicular development, we analyzed the promoter of *IFFD* and found that the DNA hypermethylation of its CGI resulted in the decreased expression of *IFFD* (Fig. 5F). Transcription factors have been verified to be closely related to the transcription of lncRNAs [34, 35]. We found that *IFFD* was activated by SP1 (Fig. 4G), which is a ubiquitous regulator of basal promoter activity [36]. SP1 mediates FSH induced the epithelial regulatory protein expression in GCs [37]. MiR-375 needs to bind with SP1 to regulate the synthesis of E2 in porcine ovaries [38]. In addition, we innovatively demonstrated that DNA methylation mediated the binding of SP1 to *IFFD* promoter using the CRISPR-dCas9. The deactivated Cas9-*TET1* and g*IFFD* vector obviously reduced the methylation status of SP1-binding site on BSP1 (Fig. 4J), but significantly elevated the expression of *IFFD* (Fig. 4K). Moreover, the hypomethylation made *IFFD* promoter more likely to be bound by SP1 (Fig. 4I).

The role of lncRNAs mainly relates to its subcellular localization [39]. We found that *IFFD* was expressed in both cytoplasm and nucleus, but was highly expressed in cytoplasm (Fig. 2G). Compared to normal ovarian GCs, miR-370 expression was declined in GCs from PCOS and correlated with the number of dominant follicles [40]. Also, miR-370 has been shown to mediate *FSHR* expression and participate in follicular formation and oocyte maturation [40, 41]. *GLI1*, a key molecule of the Hedgehog signaling pathway, is closely related to the proliferation and apoptosis of many cells and follicular growth [42–44]. In mouse follicles, *Gli1* is involved in follicular development through mediating interactions between GCs and theca cells [29, 45]. In our study, we found that *IFFD* inhibited GCs proliferation (Fig. 3F) and E2 secretion (Fig. 3K) and promoted GCs apoptosis (Fig. 3P) by sponging miR-370, leading to the increased expression of *GLI1*. A previous study has indicated that lncRNA *Neat1* knockout leads to ovarian defects by impairing luteum formation and decreasing fertility [28]. To further characterize the function of *IFFD*, we built the lentiviral for *IFFD* overexpression or knockdown, and found that *IFFD* promoted the loss of follicular blood vessels, follicular

fluid turbidity (Fig. 5D), and GCs apoptosis (Fig. 5E) in pigs. Also, *IFFD* promoted GCs apoptosis (Fig. 6H), impeded E2 secretion (Fig. 6F) and follicular development (Fig. 6G), or delayed pubertal initiation in mice (Fig. 6E).

In conclusion, we found that *DNMT1* downregulation induces the hypomethylation of *IFFD* and then promotes its transcription by recruiting the binding of SP1. *IFFD* increases *GLI1* expression by sponging miR-370, and promotes GCs apoptosis, inhibits GCs proliferation, E2 secretion, and ultimately blocks follicular development (Fig. 6I). These results indicate that *DNMT1*-mediated *IFFD* may act as a potential therapeutic strategy for regulation of the follicular development.

MATERIALS AND METHODS

Animals

Three-week-old female C57BL/6J mice ($n = 20$) obtained from Guangdong medical laboratory animal center (China) were assigned into LV-NC ($n = 5$), LV-lnc *IFFD* ($n = 5$), sh-NC ($n = 5$), and sh-lnc *IFFD* ($n = 5$) groups, randomly. The lentiviral vector that overexpression or knockdown of lnc *IFFD* (LV-lnc *IFFD* or sh-lnc *IFFD*) was synthesized by Dongze Biotechnology Co., LTD (Guangzhou, China). The lentivirus was injected in the same way as our previous study [10]. Briefly, 1×10^7 TU of lentivirus was infected into mice via intraperitoneal injection and was given once a week for 3 weeks. In this study, the pubertal initiation of mice was characterized by the opening of vaginal orifice.

Isolation and culture of GCs and follicles

More than 500 ovaries of prepubertal gilts were obtained from a large slaughterhouse, washed with PBS containing streptomycin/penicillin, and transported to the cell chamber. GCs collected from 3–5 mm follicles through syringes were cultured with DMEM containing 10–12% FBS and incubated at 37 °C and 5% CO_2. Plasmids were transfected into GCs through Lipofectamine™ 3000 (Thermo Scientific, USA). 3–5 mm antral follicles separated from ovaries were cultured with serum-free DMEM/F12 in 24-well plate and incubated at 38.5 °C and 5% CO_2. 100 ng/mL GDF9 (MCE, USA), 50 ng/mL BMP15 (MCE, USA), 100 ng/mL FSH (MCE, USA), 10 ng/mL testosterone (MCE, USA), and 0.5 μM 5-Aza-CdR were used to treat porcine GCs for 24 h.

RNA sequencing and data analysis

The porcine GCs treated with 5-Aza-CdR (named as group A), DMSO (named as group AD), *DNMT1*-siRNA (named as group D), and siRNA-NC (named as group ND) were used for RNA-seq. The quality and quantity of total RNA extracted by TRIzol were detected by Nanodrop 2000 spectrophotometer and gel electrophoresis. RNA-seq was then conducted with the Illumina Hiseq 2500. The adapter sequences paired reads in which the content of N in paired-end sequencing reads exceeds 3% of the read length and low-quality reads were removed. The cleaned reads were mapped to the Sus scrofa11.1. reference genome using HISAT2 [46], and the mapped reads were assembled and transcripts utilizing Stringtie [47]. CPC2 [48], CNCI [49], and FEELnc [50] software were used for the prediction of coding ability. Finally, the transcripts whose coding ability was not predicted by all three were selected, and the ones whose RNA length > 200 were judged to be lncRNAs. The screening criteria for differentially expressed lncRNAs is based on the FPKM value. DESeq2 [51] of R software was used to differential screening, and $|\log2FC| > 1$ and FDR < 0.05 as the cut-off.

Real-time quantitative PCR

The cDNA of samples was obtained through the RevertAid First Strand cDNA Synthesis Kit (Thermo). Quantitative PCR was conducted using SYBR Green qRT-PCR Mix (2x) (Thermo) and detected by the CFX96 Touch PCR instrument (Bio-Rad, Berkeley, USA). Glyceraldehyde phosphate dehydrogenase (*GAPDH*) or U6 was selected as endogenous control, and the $2^{-\Delta\Delta ct}$ method was applied for the analysis of expression level. The primer sequences were shown in Tables 1 and 2.

EdU assay

EdU assay was performed based on instruction of the Cell-Light™ Edu Apollo Kit (RiboBio, China). The GCs transfected with plasmids in 48-well plates after 24 h were treated with Triton X-100 for 10–15 min, EdU staining buffer for 30–45 min and Hoechst for 10–15 min. GCs were counted in three random fields per well under an inverted fluorescence microscope. The proliferation rate of GCs in each group was the ratio of EdU-labeled proliferating cells to all Hoechst-labeled cells.

Flow cytometry

Based on the instruction of the Annexin V-FITC Apoptosis Detection Kit (BioVision, USA), the GCs transfected with plasmids in 6-well plates for 24 h were resuspended with 1× Annexin V buffer, and then treated with Annexin V-FITC and PI in darkness. GCs apoptosis was analyzed through a flow cytometry (guava easyCyte, Luminex, USA), and counted as the sum of early and late apoptosis.

ELISA

ELISA was conducted according to the instruction of the mouse estrogen ELISA Kit (Enzyme-linked Biotechnology, ml063198, Shanghai, China) and porcine estrogen ELISA Kit (ml002366). Standard in different concentrations and samples were incubated with 100 μl of horse radish peroxidase for 1 h at 37 °C, and 50 μl each of substrate A and B for 15 min. The termination solution was then added to obtain OD value at 450 nm. The standard curve was drawn based on the concentration of the standard and the corresponding OD value.

Immunofluorescence, HE staining, and TUNEL assay

The prepared paraffin sections of ovaries were placed in dewaxing solution for 10–15 min and anhydrous ethanol for 15 min. The washed ovarian sections were incubated with EDTA antigen retrieval buffer and repaired in a microwave oven. A histochemical pen was used to draw a circle around the tissue of the slices, and BSA was dropped and incubated for 30 min, following incubating primary antibodies overnight and secondary antibodies for 50 min. DAPI dye solution was incubated at 37 °C in darkness for 10 min, and autofluorescence quench was treated for 5 min. The tablets were sealed with anti-fluorescence quench sealing agent. The dewaxed sections were incubated with hematoxylin for 5 min and eosin dye solution for 3 min, then dehydrated and sealed. Finally, the sections were photographed under a fluorescence microscope.

TUNEL assay was performed based on instruction of the TUNEL Apoptosis Assay Kit (Beyotime, China). Follicles which cut into paraffin sections were incubated with xylene for 10 min, ethanol for 5–10 min, and protease K for 15 min, respectively. The washed sections were incubated with TUNEL reagent for 1 h in darkness and observed under Nikon ECLIPSE Ti2 fluorescence microscope.

Bisulfite sequencing PCR (BSP)

BSP was conducted on the grounds of instruction of the EZ DNA Methylation-Gold™ Kit (ZYMO, USA). Using the purified DNA treated with CT conversion reagent as template, the corresponding fragments were amplified by BSP primer. QUMA (http://quma.cdb.riken.jp/) was used to compare the sequencing results with the corresponding original sequences and produce dot plots. Ten clones in each group were used to obtain the methylation rate. The primers were listed in Table 3.

The pdCas9-*TET1*-CD vector (dC-*TET1*, 83340, ADDGENE, USA) and sgRNA targeted to the −1261/−1254 region of *IFFD* promoter (g*IFFD*) were used to specific demethylation of the SP1-binding site on CGI. The sgRNA was synthesized by Guangzhou Dongze Biotechnology Co., LTD (China). The target sequence of sgRNA vector was GCTGGGATCCATGAGGATGC.

Chromatin Immunoprecipitation assay (ChIP)

Based on the instruction of the PierceTM ChIP kit (Thermo), the GCs treated with formaldehyde after 10–15 min were quenched by glycine. The chromatin fragments solution obtained from automatic ultrasonic crushing machine was then incubated with SP1 antibody (21962-1-AP, proteintech, Wuhan, China) and IgG antibody (12–370, Millipore) at 4 °C overnight. The purified DNA was used for real-time quantitative PCR and the primers were listed in Table 3.

FISH assay

The Ribo™ Fluorescent In Situ Hybridization Kit (RiboBio) was selected for FISH assay. The GCs cultured at 24-well plates after 24 h were treated with paraformaldehyde and Triton X-100 for 15 min, prehybridization solution for 30 min, and then incubated with *IFFD* probe mix overnight. The washed

Table 1. Primers used for qPCR in pig.

Gene name	Primer sequences (5′ to 3′)	Size (bp)	Accession number
DNMT1	F: TTCCCAGAGCCACTGTTCGC	141	NM_001032355.1
	R: GGGAAGGTCGGACATTGTGT		
DNMT3A	F: TATGAACAGGCCGTTGGCAT	189	NM_001097437.1
	R: TCAGTGCACCACAGGATGTC		
DNMT3B	F: ATCAGAGGCCGCAGATCAAG	176	NM_001348900.1
	R: GCTGGACTTTCAGACCGAGT		
PCNA	F: TCGTTGTGATTCCACCACCAT	278	NM_001291925.1
	R: TGTCTTCATTGCCAGCACATTT		
CDK1	F: AGGTCAAGTGGTAGCCATGAA	225	NM_001159304.2
	R: TCCATGAACTGACCAGGAGG		
CDK2	F: AAAAGATCGGAGAGGGCACG	121	NM_001285465.1
	R: GCAGTACTGGGTACACCCTC		
CDK4	F: CCTCCCGGTATGAACCAGTG	277	NM_001123097.1
	R: TGCTCAAACACCAGGGTCAC		
CCNA1	F: GCGCCAAGGCTGGAATCTAT	196	XM_005668339.3
	R: CCTCAGTCTCCACAGGCTAC		
CCNA2	F: GTACTGAAGGCCGGGAACTC	192	NM_001177926.1
	R: AGCTGGCCTCTTTTGAGTCT		
CCNB1	F: ACGGCTGTTAGCTAGTGGTG	236	NM_001170768.1
	R: GAGCAGTTCTTGGCCTCAGT		
CCNB2	F: TGGAAATCGAGTTACAACCAGA	151	NM_001114282.1
	R: TGGAGCCAACATTTCCATCTGT		
CCND1	F: CTTCCATGCGGAAGATCGTG	234	XM_021082686.1
	R: TGGAGTTGTCGGTGTAGATGC		
CCND2	F: TTCCCCAGTGCTCCTACTTC	259	NM_214088.1
	R: CACAACTTCTCAGCCGTCAG		
CCNE1	F: AGCCTGTGAAAACCCCTGTT	252	XM_005653265.2
	R: TCCAGAAGAATCGCTCGCAT		
CCNE2	F: GGGGGATCAGTCCTTGCATT	154	NM_001243931.1
	R: AGCCAAACATCCTGTGAGCA		
RRM1	F: CTTCAATGCTGGCACCAACC	260	XM_021062424.1
	R: TGTTTCCACCCTGATCCACG		
RRM2	F: CATCGAGACAATGCCTTGCG	233	XM_021087850.1
	R: AGGCGAAGTCGCAGTGTAAA		
CASP3	F: ACATGGAAGCAAATCAATGGAC	154	NM_214131.1
	R: TGCAGCATCCACATCTGTACC		
CASP8	F: GAGCCTGGACTACATCCCAC	283	NM_001031779.2
	R: GTCCTTCAATTCCGACCTGG		
CASP9	F: GCTGAACCGTGAGCTTTTCA	161	XM_003127618.4
	R: CCTGGCCTGTGTCCTCTAAG		
TP53	F: ACGCTTCGAGATGTTCCGAG	137	NM_213824.3
	R: TTTTATGGCGGGAGGGAGAC		
BAX	F: ACTTCCTTCGAGATCGGCTG	184	XM_013998624.2
	R: AAAGACACAGTCCAAGGCGG		
BAK1	F: CTCGTCCACATCAGAGGAGC	147	XM_013977773.2
	R: CTAGGTTCTAGGGGCAGGGT		
BID	F: ACGAGCGCATCACAAACCTA	196	NM_001030535.1
	R: GCCTCCTGGCTCTCAGAATC		
BIM	F: GAGCGGCAAGCTTCCATGAG	136	NM_001252194.1
	R: AAGAAAACAGCATTACCCTCC		
BCL2	F: GATGCCTTTGTGGAGCTGTATG	145	XM_021099593.1
	R: CCCGTGGACTTCACTTATGG		

Table 1. continued

Gene name	Primer sequences (5′ to 3′)	Size (bp)	Accession number
BCL2L1	F: TGACCACCTAGAGCCTTGGA	124	NM_214285.1
	R: CGTCAGGAACCATCGGTTGA		
MCL1	F: GAAGGCGTTAGAGACCCTGC	167	NM_001348806.1
	R: TGCCCCAGTTTGTTACTCCG		
STAR	F: CGACGTTTAAGCTGTGTGCT	136	NM_213755.2
	R: ATCCATGACCCTGAGGTTGGA		
CYP11A1	F: CTAAAACCCCTCGCCCCTTC	199	NM_214427.1
	R: GCCACATCTTCAGGGTCGAT		
CYP17A1	F: CCACACGGAATGGAGAGTCC	263	NM_214428.1
	R: TTCCCGCAGCAATTCGTTTC		
CYP19A1	F: CTGAAGTTGTGCCTTTTGCCA	139	NM_214429.1
	R: CTGAGGTAGGAAATTAGGGGC		
HSD3B1	F: ATCTGCAGGAGATCCGGGTA	216	NM_001004049.2
	R: CCTTCATGACGGTCTCTCGC		
HSD17B1	F: GTCTGGCATCTGACCCATCTC	166	NM_001128472.1
	R: CGGGCATCCGCTATTGAATC		
Lnc IFFD	F: GTCGGGCGATGCTATCAGAG	167	
	R: GGCCTTGCTAAGCCATACCT		
GLI1	F: TTCAACTCGATGACCCCACC	152	NM_001256593.1
	R: CTGTGGGGACCAGACATGAG		
SP1	F: GTTCGCTTGCCTCGTCAGC	199	XM_005652567.3
	R: CCTGAGAAAAGGCACCACCAT		
GAPDH	F: TCGGAGTGAACGGATTTGGC	189	NM_001206359.1
	R: TGACAAGCTTCCCGTTCTCC		

Table 2. Primers used for qPCR in the mouse.

Gene name	Primer sequences (5′ to 3′)	Size (bp)	Accession number
Gli1	F: GAAGGCCTGCTCCCTGAAAT	126	NM_001285785.2
	R: GCACTGCTGTCCCTAGTCAA		
Casp3	F: TGGCGTGTGCGAGATGAG	211	NM_009810.3
	R: TTGTTGTTCTCCATGGTCAC		
Bax	F: GCACGTCCACGATCAGTCAC	261	NM_007527.3
	R: CACTCGCTCAGCTTCTTGGT		
Casp8	F: CGGGAAAAGGGGATGTTGGA	202	NM_009812.2
	R: CCAACTCGCTCACTTCTTCTGA		
Pcna	F: GTGAACCTGCAGAGCATGGA	216	NM_011045.2
	R: TGGTGCTTCGAATACTAGTGC		
Ccnb1	F: AGGGTGTCTTCTCGAATCGG	154	NM_172301.3
	R: GGCTTGGAAGCAGCAGTAAC		
Ccnd1	F: GCCATCCATGCGGAAAATCG	205	NM_001379248.1
	R: GGCAGTCAAGGGAATGGTCT		
Cyp19a1	F: CCACCACTGCTTTCTTCCCAT	283	NM_007810.4
	R: CACTTCCAATCCCCATCCACA		
Hsd17b1	F: AGATTGCCAGCAGACACAACA	273	XM_006532297.3
	R: CAACAATGGTCCCTGTGCCTT		

GCs were treated with DAPI for 10 min and observed with confocal microscope (FV3000, OLYMPUS, JAPAN).

Dual-luciferase reporter gene assay

The RNA22 website (https://cm.jefferson.edu/rna22/) was used to predict the potential binding relation of *IFFD* and miR-370. The sequence of *IFFD* 3′ UTR containing the binding sites of miR-370 (lnc *IFFD*-WT) and the mutated binding site of miR-370 (lnc *IFFD*-MUT) were cloned into pmirGLO-reporter (Promega, Madison, USA) by the endonuclease sites *Sac1* and *Sall*. The GCs at 70% fusion were transfected with lnc *IFFD*-WT and lnc *IFFD*-MUT mixed with mimics NC and miR-370 mimic for 48 h, respectively. The luciferase activity reporter assay was conducted by using the Dual-Luciferase Reporter Assay System (Promega, USA) and detected by Synergy Neo2 Reader (BioTek, USA).

Table 3. Primers used for BSP and ChIP-PCR.

Primer name	Primer sequences (5′ to 3′)
BSP1	F1: AACCTCATCTGTGACTTACACAAC
	R1: CTGGATGTCACCATCAGAACCTCTC
BSP2	F2: CTCATCTTATCATTCCGAAAGCAACTG
	R2: AAGGCTCCATTGAATGATTTCC
BSP3	F3: AATGCCTTCTATAGGAACAAACCTG
	R3: CTCTGACCTGAACCAGCAGGCGCTG
SP1-ChIP-PCR	F: GGTAACAAATCTGACAGGGA
	R: ACAATTCATGGTAATGCCGGA

Table 5. Oligonucleotide sequences in this study.

Fragment name	Sequences (5′ to 3′)
MiR-370 mimic	GCCUGCUGGGGUGGAACCUGGU
MiR-370 inhibitor	ACCAGGUUCCACCCCAGCAGGC
DNMT1-siRNA	TACAGTTGTTGACAAACGAG
DNMT3A-siRNA	ACCCTTACAAAGAAGTTTACA
DNMT3B-siRNA	CTCATTTTATCTTCTAAAACT
GLI1-siRNA	CCACAGGGCAGCAGCACTA
Si-lnc IFFD	GCUCUAGCAGCUCGGACAA

Table 4. Primers used for vector construction.

Primer name	Primer sequences (5′ to 3′)
pcDNA3.1-DNMT1	F: CCAAGCTTCTGGGCCGGGATGGTACG
	R: GGGGTACCATCCCTGGTGCCAGAAACAA
pcDNA3.1-lnc IFFD	F: CCAAGCTTTCTCTTGGGAAAGGAACAAAG
	R: GGGGTACCTCCCTACACCACCTTCCTGAC
pcDNA3.1-SP1	F: CCAAGCTTCCTCAGCTGCCACCATGAGC
	R: GGGGTACCGTATGGCCCATATGTCTCTA
pGL3-lnc IFFD	F: CGACGCGTGGCCAGCTTTAAATAGGGACA
	R: CCCTCGAGCTCTCTGATAGCATCGCCCG
pGL3-BSP1	F: CGACGCGTAACCTCATCTGTGACTTACA
	R: CCCTCGAGGATGTCACCATCAGAACCTC
pGL3-BSP2	F: CGACGCGTCTCATCTTATCATTCCGAAA
	R: CCCTCGAGAAGGCTCCATTGAATGAT
pGL3-BSP3	F: CGACGCGTATGCCTTCTATAGGAACA
	R: CCCTCGAGCTCTGACCTGAACCAGCAG
lnc IFFD-WT	F: CGAGCTCTCTCTTGGGAAAGGAACAAAG
	R: GCGTCGACTCCCTACACCACCTTCCTGAC
lnc IFFD-MUT	F: AATGAGAGAGGAAAAGGTCGTCCCTTTCCAGGTATGGC
	R: GCCATACCTGGAAAGGGACGACCTTTTCCTCTCTCATT
GLI1-WT	F: CGAGCTCCAAGCACCAGAATCGGACCC
	R: GCGTCGACTCTCAAGGCGGCGAAGAGTA
GLI1-MUT	F: GTATTGGCCGCGCTGCCTGCTGGGGAGTGGTCACTGCTGC
	R: GCAGCAGTGACCACTCCCCAGCAGGCAGCGCGGCCAATAC
pcDNA3.1-EGFP	F: GGCTAGCCATGGTGAGCAAGGGCGAGGAG
	R: CAAGCTTGTTACTTGTACAGCTCGTCCA
pcDNA3.1-EGFP-MUT	F: GGCTAGCCGTGAGCAAGGGCGAGGAGCTG
	R: CAAGCTTGTTACTTGTACAGCTCGTCCA
pcDNA3.1-ORF+EGFP-MUT	F: GGCTAGCCAGCATGTTAAGGCCTGCCATG
	R: CAAGCTTGTTACTTGTACAGCTCGTCCA

Sequences underlined represent the enzyme cutting sites.

The potential binding relation of miR-370 and *GLI1* 3′ UTR was predicted at the website (http://www.targetscan.org/). The sequence of *GLI1* 3′ UTR containing the binding sites of miR-370 (*GLI1*-WT) and the mutated binding site of miR-370 (*GLI1*-MUT) were synthesized and used for plasmid construction. The GCs at 70% fusion were transfected with *GLI1*-WT and *GLI1*-MUT mixed with mimics NC and miR-370 mimic for 48 h, respectively.

Western blot analysis

The concentration of extracted total protein was determined through the BCA Protein Assay Kit (Beyotime, China). The equal proteins of each sample were electrophoresed by SDS-PAGE gels and transferred to polyvinylidene difluoride (PVDF) membranes. The PVDF membranes treated with 5% skimmed milk at 37 °C for 1 h were incubated with DNMT1 (ab188453, abcam, 1:1000), DNMT3A (32578, CST, 1:1000), DNMT3B (57868, CST, 1:1000), SP1 (21962-1-AP, proteintech, 1:5000), PCNA (10205-2-AP, proteintech, 1:2000), CCND1 (26939-1-AP, proteintech, 1:1000), CASP3 (19677-1-AP, proteintech, 1:1000), BAX (50599-2-Ig, proteintech, 1:5000), CYP19A1 (bs-0114R, bioss, 1:2000), CYP11A1 (bs-3608R, bioss, 1:2000), GLI1 (66905-1-Ig, proteintech, 1:3000) and Tubulin (ab7291, Abcam, 1:10,000) at 4 °C overnight. The washed membranes were then incubated with goat anti-mouse (ab6789, Abcam, 1:5000) or goat anti-rabbit IgG H&L (ab205718, Abcam, 1:10000) at 37 °C for 2 h. The Tanon 5200 Muti (Shanghai, China) and ImageJ were used to observe and measure the blots, respectively.

RNA pull down

According to the instruction of Pierce™ Magnetic RNA-Protein Pull-Down Kit (Thermo), the GCs were lysed using standard lysate buffers and the 3 'of the target lncRNA labeled with biotin. The labeled RNA bound to the streptavidin magnetic beads was treated with equal amount of 1× RNA capture buffer and 100 µl 1× protein-RNA-binding solution. The RNA-bound magnetic beads were treated with 100 µl Master Mix for 30–60 min, and then the RNA-binding complexes were eluted.

Full-length amplification and coding ability verification of *IFFD*

A 5′/3′-RACE Kit (Roche, USA) was used to obtain the full-length sequences of *IFFD*. Total RNA from GCs was used as the template for nested-PCR, and the corresponding products of RACE PCR were sequenced.

To verify the coding ability of *IFFD*, the Open Reading Frame (ORF) of EGFP (GFP-WT), the deleted EGFP start codon ATG (GFP-MUT), and ORF of *IFFD* with GFP-MUT were amplified and inserted into pcDNA3.1 by using the *NheI* and *HindIII* restriction sites. All primers used for vector construction were listed in Table 4 and oligonucleotide sequences were listed in Table 5.

Statistical analysis

All data are shown as mean ± standard deviation from at least three independent replicate experiments. Differences were analyzed by Student's *t*-test, and $P < 0.05$ or $P < 0.01$ represents statistically significant.

DATA AVAILABILITY

The RNA-seq data supporting the results of this study have been deposited in the NCBI BioProject database under accession number PRJNA906921.

REFERENCES

1. McGee EA, Hsueh AJ. Initial and cyclic recruitment of ovarian follicles. Endocr Rev. 2000;21:200–14.
2. Matsuda F, Inoue N, Manabe N, Ohkura S. Follicular growth and atresia in mammalian ovaries: regulation by survival and death of granulosa cells. J Reprod Dev. 2012;58:44–50.
3. Kumariya S, Ubba V, Jha RK, Gayen JR. Autophagy in ovary and polycystic ovary syndrome: role, dispute and future perspective. Autophagy. 2021;17:2706–33.
4. Richards JS, Ren YA, Candelaria N, Adams JE, Rajkovic A. Ovarian follicular theca cell recruitment, differentiation, and impact on fertility: 2017 update. Endocr Rev. 2018;39:1–20.
5. Jin M, Yu Y, Huang H. An update on primary ovarian insufficiency. Sci China Life Sci. 2012;55:677–86.
6. Richards JS. From follicular development and ovulation to ovarian cancers: an unexpected journey. Vitam Horm. 2018;107:453–72.
7. Azziz R. PCOS in 2015: new insights into the genetics of polycystic ovary syndrome. Nat Rev Endocrinol. 2016;12:183.
8. De Vos M, Devroey P, Fauser BCJM. Primary ovarian insufficiency. Lancet. 2010;376:911–21.
9. Visser JA, Schipper I, Laven JSE, Themmen APN. Anti-Mullerian hormone: an ovarian reserve marker in primary ovarian insufficiency. Nat Rev Endocrinol. 2012;8:331–41.
10. Zhou X, He Y, Li N, Bai G, Pan X, Zhang Z, et al. DNA methylation mediated RSPO2 to promote follicular development in mammals. Cell Death Dis. 2021;12:653.
11. Yeung CK, Wang G, Yao Y, Liang J, Tenny Chung CY, Chuai M, et al. BRE modulates granulosa cell death to affect ovarian follicle development and atresia in the mouse. Cell Death Dis. 2017;8:e2697.
12. Khristi V, Chakravarthi VP, Singh P, Ghosh S, Pramanik A, Ratri A, et al. ESR2 regulates granulosa cell genes essential for follicle maturation and ovulation. Mol Cell Endocrinol. 2018;474:214–26.
13. Zhang H, Luo Q, Lu X, Yin N, Zhou D, Zhang L, et al. Effects of hPMSCs on granulosa cell apoptosis and AMH expression and their role in the restoration of ovary function in premature ovarian failure mice. Stem Cell Res Ther. 2018;9:20.
14. Pan Z, Zhang J, Li Q, Li Y, Shi F, Xie Z, et al. Current advances in epigenetic modification and alteration during mammalian ovarian folliculogenesis. J Genet Genomics. 2012;39:111–23.
15. Liu YN, Qin Y, Wu B, Peng H, Li M, Luo H, et al. DNA methylation in polycystic ovary syndrome: emerging evidence and challenges. Reprod Toxicol. 2022;111:11–19.
16. He C, Wang K, Gao Y, Wang C, Li L, Liao Y, et al. Roles of noncoding RNA in reproduction. Front Genet. 2021;12:777510.
17. Herman JG, Baylin SB. Mechanisms of disease: gene silencing in cancer in association with promoter hypermethylation. N Engl J Med. 2003;349:2042–54.
18. Lomniczi A, Loche A, Castellano JM, Ronnekleiv OK, Bosch M, Kaidar G, et al. Epigenetic control of female puberty. Nat Neurosci. 2013;16:281–9.
19. Kawai T, Richards JS, Shimada M. The cell type-specific expression of Ihcgr in mouse ovarian cells: evidence for a DNA-demethylation-dependent mechanism. Endocrinology. 2018;159:2062–74.
20. Kawai T, Richards JS, Shimada M. Large-scale DNA demethylation occurs in proliferating ovarian granulosa cells during mouse follicular development. Commun Biol. 2021;4:1334.
21. Jandura A, Krause HM. The new RNA world: growing evidence for long noncoding RNA functionality. Trends Genet. 2017;33:665–76.
22. Tay Y, Rinn J, Pandolfi PP. The multilayered complexity of ceRNA crosstalk and competition. Nature. 2014;505:344–52.
23. Salmena L, Poliseno L, Tay Y, Kats L, Pandolfi PP. A ceRNA hypothesis: the Rosetta Stone of a hidden RNA language? Cell. 2011;146:353–8.
24. Zhang D, Tang HY, Tan L, Zhao DM. MALAT1 is involved in the pathophysiological process of PCOS by modulating TGFbeta signaling in granulosa cells. Mol Cell Endocrinol. 2020;499:110589.
25. Zhao J, Xu J, Wang W, Zhao H, Liu H, Liu X, et al. Long non-coding RNA LINC-01572:28 inhibits granulosa cell growth via a decrease in p27 (Kip1) degradation in patients with polycystic ovary syndrome. Ebiomedicine. 2018;36:526–38.
26. Geng X, Zhao J, Huang J, Li S, Chu W, Wang WS, et al. lnc-MAP3K13-7:1 inhibits ovarian GC proliferation in PCOS via DNMT1 downregulation-mediated CDKN1A promoter hypomethylation. Mol Ther. 2021;29:1279–93.
27. Adriaens C, Rambow F, Bervoets G, Silla T, Mito M, Chiba T, et al. The long noncoding RNA NEAT1_1 is seemingly dispensable for normal tissue homeostasis and cancer cell growth. RNA. 2019;25:1681–95.
28. Nakagawa S, Shimada M, Yanaka K, Mito M, Arai T, Takahashi E, et al. The lncRNA Neat1 is required for corpus luteum formation and the establishment of pregnancy in a subpopulation of mice. Development. 2014;141:4618–27.
29. Wijgerde M, Ooms M, Hoogerbrugge JW, Grootegoed JA. Hedgehog signaling in mouse ovary: Indian hedgehog and desert hedgehog from granulosa cells induce target gene expression in developing theca cells. Endocrinology. 2005;146:3558–66.
30. Dewailly D, Robin G, Peigne M, Decanter C, Pigny P, Catteau-Jonard S. Interactions between androgens, FSH, anti-Mullerian hormone and estradiol during folliculogenesis in the human normal and polycystic ovary. Hum Reprod Update. 2016;22:709–24.
31. Chen J, Wu L, Xu H, Cheng S. 5-Aza-CdR regulates RASSF1A By inhibiting DNMT1 to affect colon cancer cell proliferation, migration and apoptosis. Cancer Manag Res. 2019;11:9517–28.
32. Lu C, Wei Y, Wang X, Zhang Z, Yin J, Li W, et al. DNA-methylation-mediated activating of lncRNA SNHG12 promotes temozolomide resistance in glioblastoma. Mol Cancer. 2020;19:28.
33. Ma Y, Yang Y, Wang F, Moyer MP, Wei Q, Zhang P, et al. Long non-coding RNA CCAL regulates colorectal cancer progression by activating Wnt/beta-catenin signalling pathway via suppression of activator protein 2alpha. Gut. 2016;65:1494–504.
34. Sang B, Zhang YY, Guo ST, Kong LF, Cheng Q, Liu GZ, et al. Dual functions for OVAAL in initiation of RAF/MEK/ERK prosurvival signals and evasion of p27-mediated cellular senescence. Proc Natl Acad Sci USA. 2018;115:E11661–E11670.
35. Yu T, Zhao Y, Hu Z, Li J, Chu D, Zhang J, et al. MetaLnc9 facilitates lung cancer metastasis via a PGK1-activated AKT/mTOR pathway. Cancer Res. 2017;77:5782–94.
36. Philipsen S, Suske G. A tale of three fingers: the family of mammalian Sp/XKLF transcription factors. Nucleic Acids Res. 1999;27:2991–3000.
37. Sekiguchi T, Mizutani T, Yamada K, Yazawa T, Kawata H, Yoshino M, et al. Transcriptional regulation of the epiregulin gene in the rat ovary. Endocrinology. 2002;143:4718–29.
38. Yu C, Li M, Wang Y, Liu Y, Yan C, Pan J, et al. MiR-375 mediates CRH signaling pathway in inhibiting E2 synthesis in porcine ovary. Reproduction. 2016;153:63–73.
39. Carlevaro-Fita J, Johnson R. Global positioning system: understanding long noncoding RNAs through subcellular localization. Mol Cell. 2019;73:869–83.
40. Cirillo F, Catellani C, Lazzeroni P, Sartori C, Nicoli A, Amarri S, et al. MiRNAs regulating insulin sensitivity are dysregulated in polycystic ovary syndrome (PCOS) ovaries and are associated with markers of inflammation and insulin sensitivity. Front Endocrinol. 2019;10:879.
41. Casarini L, Crepieux P. Molecular mechanisms of action of FSH. Front Endocrinol. 2019;10:305.
42. Jing D, Li C, Yao K, Xie X, Wang P, Zhao H, et al. The vital role of Gli1(+) mesenchymal stem cells in tissue development and homeostasis. J Cell Physiol. 2021;236:6077–89.
43. Russell MC, Cowan RG, Harman RM, Walker AL, Quirk SM. The hedgehog signaling pathway in the mouse ovary. Biol Reprod. 2007;77:226–36.
44. Galvin KE, Ye H, Erstad DJ, Feddersen R, Wetmore C. Gli1 induces G2/M arrest and apoptosis in hippocampal but not tumor-derived neural stem cells. Stem Cells. 2008;26:1027–36.

45. Liu C, Peng J, Matzuk MM, Yao HH. Lineage specification of ovarian theca cells requires multicellular interactions via oocyte and granulosa cells. Nat Commun. 2015;6:6934.
46. Kim D, Langmead B, Salzberg SL. HISAT: a fast spliced aligner with low memory requirements. Nat Methods. 2015;12:357–60.
47. Pertea M, Pertea GM, Antonescu CM, Chang TC, Mendell JT, Salzberg SL. StringTie enables improved reconstruction of a transcriptome from RNA-seq reads. Nat Biotechnol. 2015;33:290–5.
48. Kang YJ, Yang DC, Kong L, Hou M, Meng YQ, Wei L, et al. CPC2: a fast and accurate coding potential calculator based on sequence intrinsic features. Nucleic Acids Res. 2017;45:W12–W16.
49. Sun L, Luo H, Bu D, Zhao G, Yu K, Zhang C, et al. Utilizing sequence intrinsic composition to classify protein-coding and long non-coding transcripts. Nucleic Acids Res. 2013;41:e166.
50. Wucher V, Legeai F, Hedan B, Rizk G, Lagoutte L, Leeb T, et al. FEELnc: a tool for long non-coding RNA annotation and its application to the dog transcriptome. Nucleic Acids Res. 2017;45:e57.
51. Love MI, Huber W, Anders S. Moderated estimation of fold change and dispersion for RNA-seq data with DESeq2. Genome Biol. 2014;15:550.

ACKNOWLEDGEMENTS

This project was supported by the earmarked fund for China Agriculture Research System (CARS-35), the National Natural Science Foundation of China (32072694), the Guangdong Basic and Applied Basic Research Foundation (2021A1515012396), and the Science and Technology Project of Guangzhou (202002030071).

AUTHOR CONTRIBUTIONS

XZ, ZZ, HZ, JL, and XY conceived the study. XZ, YH, GB, HQ, and YL conducted in vivo experiments. XZ, YH, BH, and NL conducted in vitro experiments. XZ and XP conducted the RNA-seq data analysis. XZ summarized results and wrote the manuscript.

COMPETING INTERESTS

The authors declare no competing interests.

ETHICS APPROVAL

All experiments were conducted with strict reference to the Regulations for Administration of Affairs Concerning Experimental Animals, and approved by the Animal Care and Use Committee of South China Agricultural University with approval number: SYXK 2019-0136.

ADDITIONAL INFORMATION

Supplementary information The online version contains supplementary material available at https://doi.org/10.1038/s41418-022-01103-y.

Correspondence and requests for materials should be addressed to Jiaqi Li or Xiaolong Yuan.